26. Crystal Growth From the Vapor Phase

Experiment MA-085

H. Wiedemeier,[a†] H. Sadeek,[a] F. C. Klaessig,[a] M. Norek,[a] and R. Santandrea[a]

ABSTRACT

The positive effects of microgravity on crystal quality and fundamental properties of the vapor transport reaction were established by analyzing the results of three transport experiments on multicomponent systems performed during the Apollo-Soyuz mission. The systems employed, consisting of germanium selenide, tellurium, germanium tetraiodide (transport agent), germanium monosulfide, germanium tetrachloride (transport agent), and argon (inert atmosphere), were

1. System A: $GeSe_{0.99}Te_{0.01} - GeI_4$
2. System B: $GeS_{0.98}Se_{0.02} - GeCl_4$
3. System C: $GeS - GeCl_4 - Ar$

The crystallographic analysis is based on a direct comparison of space-grown and ground-based (prototype) crystals, by means of X-ray diffraction, microprobe, microscopic, and chemical etching techniques. The results demonstrate a considerable improvement of the space-grown crystals in terms of chemical and crystalline homogeneity, surface morphology, and bulk perfection relative to ground specimens. The confirmation of greater mass transport rates than predicted for a microgravity environment by existing vapor transport models is of basic scientific and practical importance for the improvement of transport models and techniques on Earth and for the development of a transport model for space conditions. The internal consistency and agreement between the Apollo-Soyuz Test Project and Skylab results obtained for different compounds, transport agents, and temperature gradients strongly support the validity of these observations. The combined findings of improved crystal quality and high mass transport rates are of technological significance for space-processing applications.

INTRODUCTION

Crystal growth by chemical vapor transport is of technological importance for the production of bulk- and layer-type single crystalline materials used in various electronic devices. It is well known that the performance characteristics of electronic materials are critically dependent on the degree of chemical homogeneity and crystalline perfection. These material properties are affected by the transport and growth conditions of a given chemical system. Complete control of these growth parameters under ground-based conditions is limited because of the presence of gravity-driven convection. Under otherwise optimal growth conditions on Earth, convective interference with the transport process causes crystalline imperfections.

Crystal growth in a microgravity environment in the absence of convective interference should produce crystals of improved quality and yield fundamental data for the vapor transport process. These expectations were confirmed by the results of Skylab Experiment M556 (Vapor Growth of IV-VI Compounds). In the Skylab experiments

[a]Rensselaer Polytechnic Institute.

[†]Principal Investigator.

(refs. 26-1 and 26-2), representative compounds of Group IV-VI materials, germanium selenide (GeSe) and germanium telluride (GeTe), were transported with germanium tetraiodide (GeI_4) as a transport agent. The single crystals grown in space are of considerably improved structural perfection compared to corresponding ground-based specimens. The second major result of the Skylab studies is the observation of greater mass transport rates in a microgravity environment than predicted for a diffusion-type transport process. Because of the far-reaching scientific and technological implications of the preceding observations, the Skylab results served as a basis for the definition of the Apollo-Soyuz Test Project (ASTP) experiments. The primary objectives of the ASTP crystal growth by vapor transport experiment were to extend and generalize microgravity crystal growth for a class of compounds and to characterize the unexpected gas motion observed during Skylab missions. For this purpose, new compounds and solid solutions were transported with different transport agents in higher temperature gradients. In addition, an inert atmosphere was used in one of the transport ampoules. Details of the experimental design and chemical systems are discussed subsequently.

This report is based on the current analysis of three transport experiments performed in space. The data reveal improved crystalline perfection for the space-grown material compared to ground-based samples. These results confirm the Skylab observations and extend the conclusions drawn to more complex systems. In addition, the mass transport rates observed in space are considerably greater than predicted by theory. The latter results not only confirm Skylab data, but provide experimental evidence for the cause of the higher than expected mass fluxes.

Because of the technological importance of single crystals for solid-state devices and because of their high yield-to-weight ratio, crystal growth by vapor transport is a primary candidate for space-processing applications. A definite purpose of the ground-based and microgravity transport studies is to provide the scientific and technical basis for actual space manufacturing. In addition, knowledge gained from these space experiments will be of practical use for the improvement of crystal growth techniques on Earth.

GROUND-BASED STUDIES

Basic Theory

In a chemical transport reaction (ref. 26-3), a gaseous (g) transport agent $B(g)$ reacts at a given temperature with the solid (s) source material $A(s)$ to form exclusively gaseous products $C(g)$. This process is represented by the following reaction.

$$xA(s) + yB(g) = zC(g) + \text{---} \qquad (26\text{-}1)$$

The number of different gaseous products formed depends on the particular chemical system. The vapor species migrate in the reaction vessel from the source to the condensation region, where, at a different temperature, the reverse reaction occurs with formation of the solid. The necessary concentration gradient is established by means of a temperature gradient, which yields different equilibrium constants for the reaction of equation (26-1) and, thus, yields different partial pressures of the gaseous species in the source and condensation zones of the system. According to equation (26-1) the solid A is transported via the gas phase by means of a chemical reaction; this is distinctly different from transport by sublimation. Under optimal experimental conditions, well-defined single crystals of the source material are obtained by the condensation reaction. Depending on the thermodynamic properties of the transport reaction, a chemical transport can occur from high to low temperature or vice versa. This aspect is of practical importance with respect to the choice of transport agent and condensation temperature. The transport reaction is performed in evacuated, sealed ampoules of fused silica that are conventionally subjected to the desired temperature gradient in a horizontal, two-zone, tubular resistance furnace.

The migration of gas phase species can be described by diffusion and by gravity-driven convection. In a gravitational field and temperature gradient, both transport modes occur simultaneously. It is a unique feature of the vapor transport technique to select experimental conditions so that one or the other mode can be predominant. Under ground-based conditions, the convective contribution to the overall transport process can be minimized but not eliminated. Based on existing models for diffusive and convective gas motion (ref. 26-3), the material flux from the source to the condensation region is affected by the pressure in the transport ampoule. At very low pressures of transport agent, the mass transport rate is controlled by the rate of the heterogeneous solid-gas phase reaction in the source or the condensation region, or both. Under these conditions, the material flux is proportional to the concentration of transport agent. At medium pressures, the transport rate is inversely proportional to the total pressure. The overall transport is diffusion controlled in this range. At higher pressures, the material flux increases with increasing total pressure, indicating the predominance of the convective transport mode. For the conditions of the diffusion- and convection-controlled transport modes, the heterogeneous solid-gas phase reactions in the source and condensation zones are fast.

Transport Properties of Group IV-VI Compounds

Mass transport rate studies on GeTe (ref. 26-4) and GeSe (ref. 26-5) confirmed the general shape of flux as a function of total pressure curves predicted by the previously described models. Details of the experimental procedures and results have been discussed in references 26-4 and 26-5. The most important observation of these studies is the decrease in crystal perfection with increasing contribution of the convective component to the overall transport process. Transport studies in the Rensselaer Polytechnic Institute (RPI) laboratory on germanium monosulfide (GeS) using germanium tetrachloride ($GeCl_4$) as a transport agent and different temperature gradients show the diffusion- and convection-controlled transport regimes in agreement with those of the preceding systems (refs. 26-4 and 26-5). In particular, the changes in crystal morphology and habit of GeS as a function of transport mode reveal the negative effects of convective interference on crystal quality. The previously described ground-based studies and the solid-solution properties of these binary systems led to the definition of mixed systems for two of the three transport experiments performed during the ASTP mission. The chemical composition of the mixed systems is given by the formulas $GeSe_{0.99}Te_{0.01}$ (system A) and $GeS_{0.98}Se_{0.02}$ (system B), respectively, where the decimal subscripts are weight percentages of the compounds and of the elements tellurium (Te) and selenium (Se). The third transport ampoule (system C) contained GeS and a mixture of $GeCl_4$ and argon (Ar). In the RPI laboratory, quantitative mass transport rate studies in terms of flux as a function of pressure were performed on these systems in the temperature gradient 877→780 K (604°→507° C). The transport agent was GeI_4 for system A and $GeCl_4$ for systems B and C. The flux is calculated from the quantity of crystals recovered, the cross section of the ampoule, and the duration of the experiment. The pressure is computed for the mean temperature of the gradient from the amount of transport agent added, assuming ideal conditions and use of $GeI_4(g)$ or $GeCl_4(g)$, respectively.

In system C, the partial pressure of argon in the ampoule was approximately twice the pressure of the transport agent $GeCl_4$. In figure 26-1, the system C flux is plotted as a function of transport-agent pressure to be consistent with systems A and B. For comparative purposes, the flux results of the GeS-$GeCl_4$ system without argon also are included in figure 26-1.

The flux curves of all systems have the same shape as those observed earlier (ref. 26-5). The diffusion-controlled region at lower pressures shows a decrease in flux with increasing pressure. The range of predominantly convective transport is characterized by an increase in flux with increasing pressure.

The leveling of the flux curve for system A at higher pressures is due to the precipitation of the

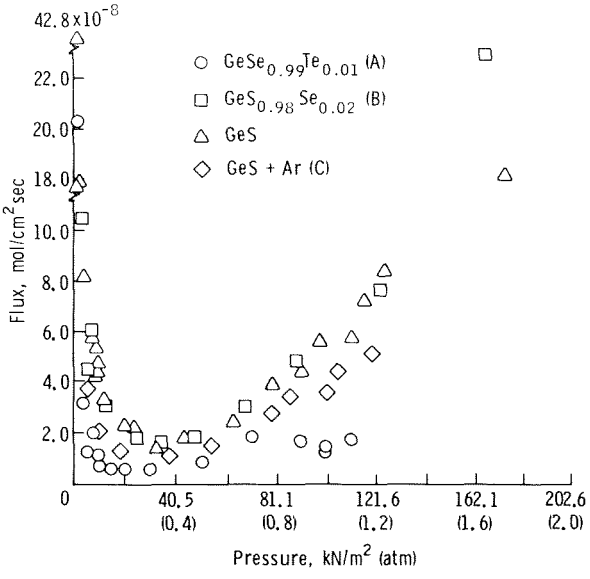

FIGURE 26-1.—Mass transport rates in terms of flux as a function of transport-agent pressure for the temperature gradient 877 → 780 K (604° → 507° C) determined under ground-based conditions.

transport agent, thus establishing a constant saturation pressure in the ampoule. The flux curves in figure 26-1, determined in the RPI laboratory, serve as a basis for the evaluation of the space experiments. For the direct comparison of mass transport rates and crystals obtained on Earth and in space, a set of three ampoules containing the same amounts of starting materials and transport agent as the corresponding ampoules used in the ASTP mission were processed in the prototype furnace. This furnace and the prototype transport conditions were identical to the furnace and conditions used in space, except for gravity.

EXPERIMENTAL ASTP PROCEDURES

Apparatus

The transport experiments were performed in the multipurpose electric furnace, which consisted essentially of a cylindrical furnace chamber and an instrumentation compartment. The furnace chamber contained three tubular reaction cavities for the individual metal cartridges and quartz ampoules discussed subsequently. Because the furnace was heated resistively in one zone at the source region, the desired temperature gradient and stability were achieved by heat shields surrounding the quartz ampoules in the metal cartridges and by appropriate heat shields in the furnace. The temperature gradient employed for those experiments in space was 877→780 K (604°→507° C) with a shallow gradient in the hot zone and a nearly linear gradient between the hot and cold zones of the reaction chamber. During the performance of the transport experiments, the furnace temperatures were constantly monitored at the outside of the metal cartridges in the hot and cold zones. The difference between furnace and actual ampoule temperatures was calibrated under identical ground-based conditions by using thermocouples.

Ampoule and Sample Preparation

The transport ampoules were made of fused silica tubing of 13.7 mm inner diameter and 150 mm length. Near the rounded end, the ampoules contained two thin silica rods to hold the source material in place. The other ampoule end was sealed after loading at a pressure of 0.1333 mN/m^2 (10^{-6} torr) or less. Before loading, the cleaned ampoules (refs. 26-4 and 26-5) were outgassed at a temperature of approximately 1273 K (1000° C) and a pressure of 0.1333 mN/m^2 (10^{-6} torr) for 10 hours. The polycrystalline starting materials were synthesized by the repeated annealing at a temperature of approximately 873 K (600° C) of stoichiometric mixtures of the binary compounds GeS, GeSe, and GeTe. The compounds were prepared from high-purity elements (99.999 percent) by annealing and subsequent sublimation of the product (refs. 26-4 and 26-5). The crystallographic identity of all materials was established by means of X-ray diffraction techniques. High-purity GeI_4 (99.999 percent) and $GeCl_4$ (99.999 percent) were used as transport agents. Ultra-high-purity argon was used as inert gas in one system. The ampoule designated 3A in this experiment contained 1.50 g of $GeSe_{0.99}Te_{0.01}$ and 123.5 mg of GeI_4. Ampoule 3B was loaded with 1.50 g of $GeS_{0.98}Se_{0.02}$ and 59.1

mg of $GeCl_4$. The third ampoule (3C) contained 1.50 g of GeS, 61.8 mg of $GeCl_4$, and 193.53 kN/m^2 (1.91 atm) of argon at the mean temperature of the gradient. The ampoules used for the ground-based prototype tests (2A, 2B, and 2C) were of the same dimensions and contents.

The chemical transport reactions for the binary compounds are shown in the following equations.

$$GeSe(s) + GeI_4(g) = 2\ GeI_2(g) + 0.5\ Se_2(g) \qquad (26\text{-}2)$$

$$GeTe(s) + GeI_4(g) = 2\ GeI_2(g) + 0.5\ Te_2(g) \qquad (26\text{-}3)$$

$$GeS(s) + GeCl_4(g) = 2\ GeCl_2(g) + 0.5\ S_2(g) \qquad (26\text{-}4)$$

The experimental conditions for the ASTP mission are summarized as follows for a temperature gradient of 877 → 780 K (604° → 507° C).

$GeSe_{0.99}Te_{0.01}$ (3A) $P(GeI_4(g)) = 70.93\ kN/m^2$ (0.70 atm)

$GeS_{0.98}Se_{0.02}$ (3B) $P(GeCl_4(g)) = 95.25\ kN/m^2$ (0.94 atm)

GeS (3C) $P(GeCl_4(g)) = 97.27\ kN/m^2$ (0.96 atm)

$P(Ar) = 193.53\ kN/m^2$ (1.91 atm)

where P indicates component gas pressure. The transport reactions of the mixed systems are analogous. The total pressures in terms of $GeI_4(g)$ or $GeCl_4(g)$ are calculated for the mean temperature of the gradient and for ideal gas conditions. The partial pressure of argon in ampoule 3C is twice the pressure of the transport agent $GeCl_4$. Thus, the total pressure in ampoule 3C is approximately three times the pressure in ampoule 3B.

Heating Cycle and Return of Ampoules

The transport ampoules were enclosed in hermetically sealed metal cartridges, which were inserted into the multipurpose furnace by the astronauts. Details of the cartridges are described in reference 26-1. After a heatup period of approximately 2 hours, the desired temperature gradient was achieved and maintained for 16 hours. Following termination of the experiment, cooling of the cartridges to ambient temperatures occurred over a period of approximately 4 hours, during which a helium quench was used.

Examination of the opened cartridges at the NASA George C. Marshall Space Flight Center revealed that none of the ampoules had any mechanical damage and that the residual source material in all ampoules was firmly attached to the ampoule wall in the source region. The ampoules were brought to the RPI laboratory for analysis of these experiments.

RESULTS AND DISCUSSION

The analysis of the transport experiments performed on the ASTP mission is based on X-ray diffraction, microprobe, microscopic, and chemical etching techniques and on mass transport rate measurements. The current results are summarized as follows.

Crystallographic Identification of Transport Products

The crystallographic identification of space-grown crystals was established by means of Debye-Scherrer and Laue X-ray diffraction techniques. For the Debye-Scherrer method, randomly selected crystals were finely powdered, sealed in thin-walled glass capillaries, and exposed to copper (Cu) Kα radiation in a 114.59-mm-diameter X-ray camera. For the Laue method, individual single-crystal platelets were mounted on the crystal holder of a conventional Laue camera and exposed to Cu Kα radiation. The results in terms of lattice parameters (Debye-Scherrer) and crystallographic orientation of as-grown predominant faces (Laue) are summarized in table 26-I together with corresponding data for ground-based (prototype) crystals.

A comparison of the data in table 26-I shows that the lattice constants of the respective systems

TABLE 26-I.—*Crystallographic Parameters of Ground-Based and ASTP Space-Grown Crystals*

Location	Lattice parameter, nm (Å)			Orientation
	a_0	b_0	c_0	
$GeSe_{0.99}Te_{0.01}$ (A)				
Ground	0.4385 (4.385) ± 0.0008 (0.008)	0.3838 (3.838) ± 0.0007 (0.007)	1.0791 (10.791) ± 0.0019 (0.019)	(001)
Space	0.4386 (4.386) ± 0.0008 (0.008)	0.3839 (3.839) ± 0.0007 (0.007)	1.0793 (10.793) ± 0.0020 (0.020)	(001)
$GeS_{0.98}Se_{0.02}$ (B)				
Ground	0.4301 (4.301) ± 0.0009 (0.009)	0.3651 (3.651) ± 0.0008 (0.008)	1.0431 (10.431) ± 0.0020 (0.020)	(001)
Space	0.4302 (4.302) ± 0.0012 (0.012)	0.3652 (3.652) ± 0.0010 (0.010)	1.0432 (10.432) ± 0.0022 (0.022)	(001)
GeS (C)				
Ground	0.4299 (4.299) ± 0.0008 (0.008)	0.3649 (3.649) ± 0.0007 (0.007)	1.0428 (10.428) ± 0.0019 (0.019)	(001)
Space	0.4301 (4.301) ± 0.0006 (0.006)	0.3651 (3.651) ± 0.0005 (0.005)	1.0430 (10.430) ± 0.0015 (0.015)	(001)

are in excellent agreement. There is no change in the orientation of predominant native faces of single crystals. Within the detection limits of X-ray diffraction techniques, there is no measurable effect of microgravity on the crystallographic parameters of space-grown crystals. The preceding results are expected in view of the relative magnitude of chemical bonding and gravitational forces.

Transmission Laue photographs of $GeSe_{0.99}Te_{0.01}$ ground (2A) and space (3A) crystals indicate considerable differences, as shown in figure 26-2. The diffraction pattern of the ground-based crystal (fig. 26-2(a)) reveals striations and multiplicity of individual diffraction spots. This condition indicates a high degree of strain and structural inhomogeneities of the ground specimen. The Laue pattern of the space crystal (fig. 26-2(b)) reveals the twofold symmetry of the predominant (001)-oriented growth face. The considerably better defined diffraction spots indicate improved crystallographic perfection compared to the ground-based sample.

Corresponding diffraction patterns of $GeS_{0.98}Se_{0.02}$ ground (2B) and space (3B) crystals in figure 26-3 demonstrate a pronounced improvement in crystallinity of the space sample (fig. 26-3(b)) relative to the ground specimen (fig. 26-3(a)). The rather well-defined diffraction spots of the space crystal (fig. 26-3(b)) reveal a considerable degree of crystallographic perfection, which has not been observed for ground crystals obtained under these conditions.

Laue diffraction patterns of GeS ground (2C) and space (3C) crystals grown in the presence of argon indicate in both cases some degree of strain (figs. 26-4(a) and 26-4(b)). Since crystals obtained under these conditions are considerably thinner than those of systems A and B, it is presently difficult to decide whether the observed strain is caused by mechanical handling of the sample or by the inclusion of argon into the crystal lattice.

The combined results of the diffraction studies for systems A and B demonstrate the distinctly improved structural homogeneity and perfection of the crystals obtained in a microgravity environment.

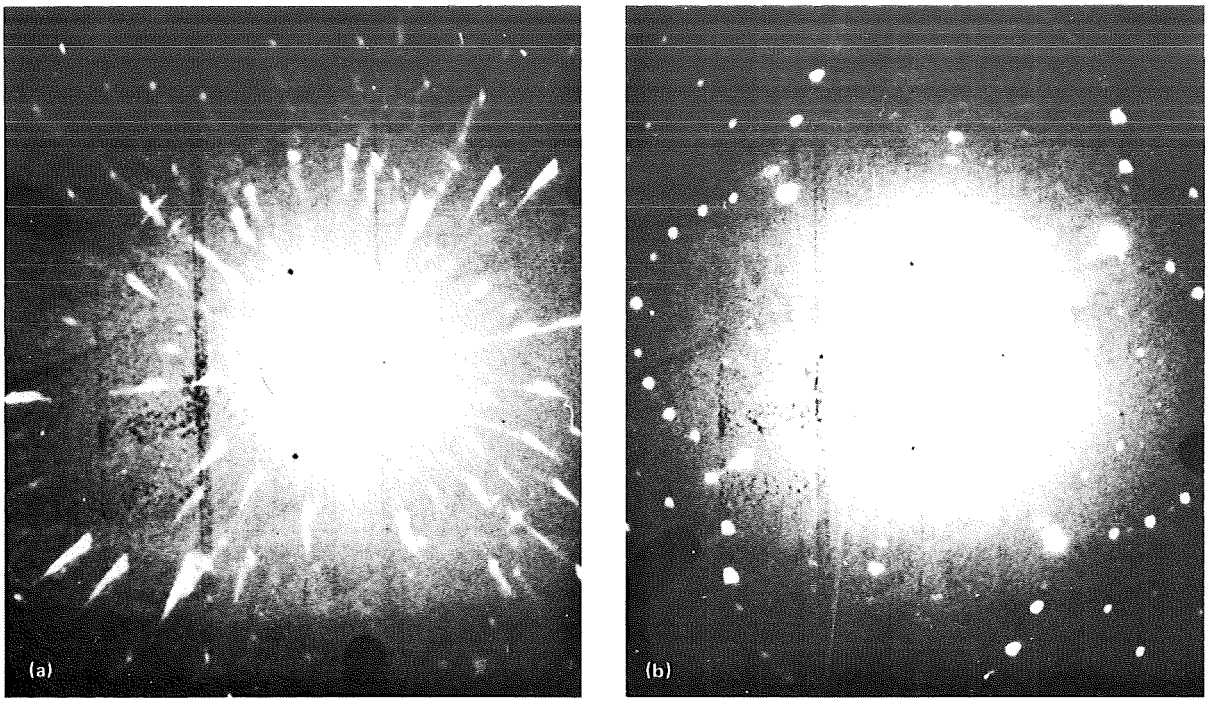

FIGURE 26-2.—Laue X-ray diffraction transmission photographs of (001)-oriented $GeSe_{0.99}Te_{0.01}$ (system A) single-crystal platelets. (a) Ground-based (prototype). (b) Space-grown.

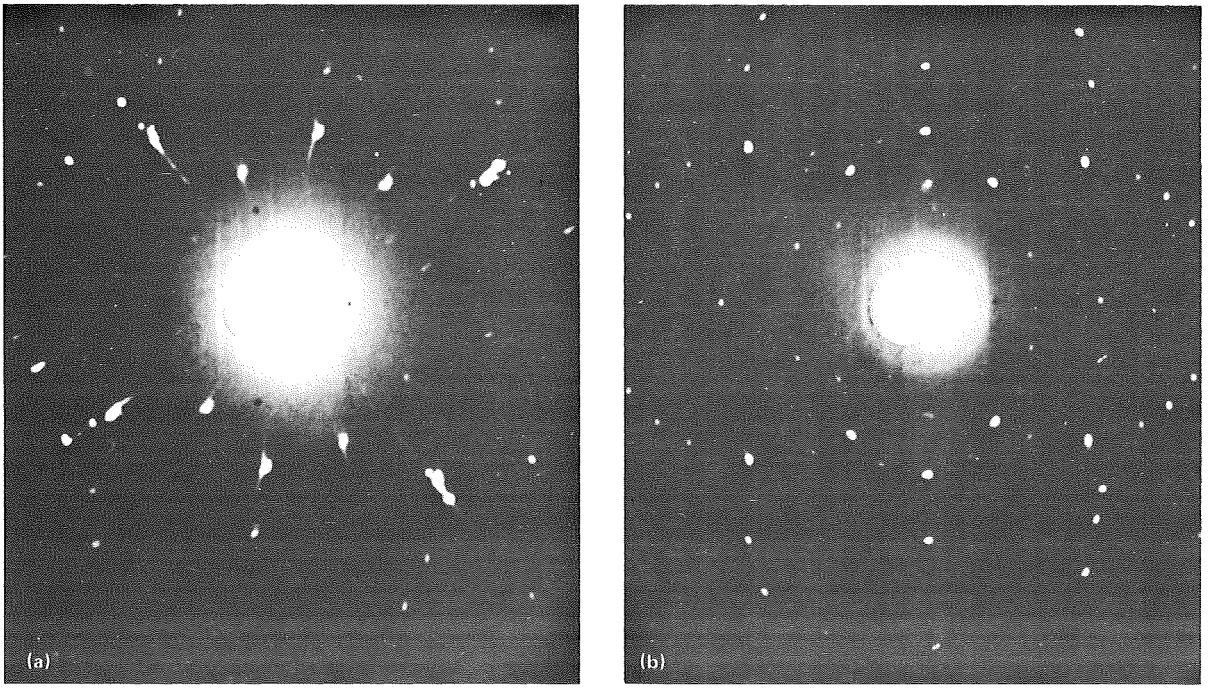

FIGURE 26-3.—Laue X-ray diffraction transmission photographs of (001)-oriented $GeS_{0.98}Se_{0.02}$ (system B) single-crystal platelets. (a) Ground-based (prototype). (b) Space-grown.

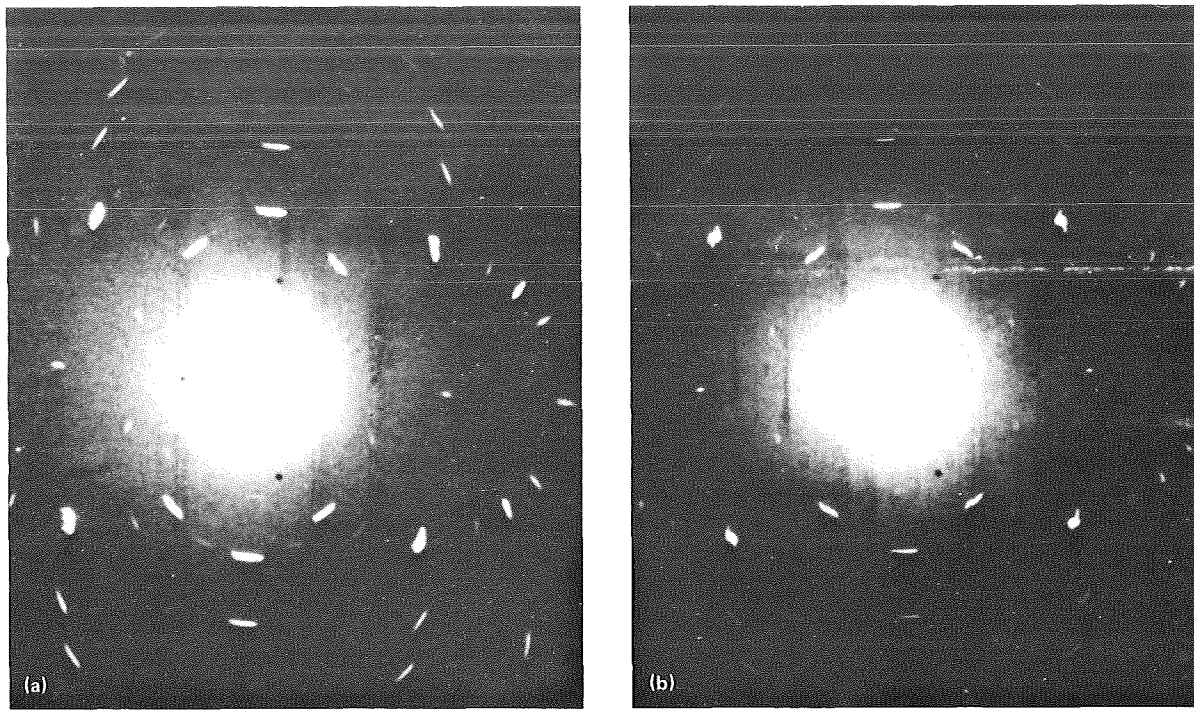

FIGURE 26-4.—Laue X-ray diffraction transmission photographs of (001)-oriented GeS (system C) single-crystal platelets. (a) Ground-based (prototype). (b) Space-grown.

Chemical Homogeneity of Crystals

To examine the chemical homogeneity of the solid solutions (systems A and B), the distribution of Te in GeSe (A) and of Se in GeS (B) was determined using an electron microprobe analyzer. For this purpose, cleaved faces of ground-based (prototype) and space-grown crystals were used. The relative concentration of Te (in GeSe) and of Se (in GeS) was measured along three directions parallel to the a-axis and the b-axis of the (001)-oriented crystal platelet. Along each direction, intensity measurements were performed at several locations. The results are summarized in table 26-II. The individual data listed are the averages of points along a given direction. The error limits represent the maximum deviation in atomic concentration of individual points from the mean value for all points along that direction. Stoichiometric GeTe and GeSe, respectively, were used as reference samples.

Based on the relative magnitude of the deviations in concentration from the average values, the distribution of Te in the solid solution of starting composition $GeSe_{0.99}Te_{0.01}$ is considerably more homogeneous in the space-grown crystal (3A) than in the ground-based crystal (2A). The differences in homogeneity are about one order of magnitude. The corresponding improvement in the distribution of Se in the space crystal (3B) compared to the ground specimen (2B) for the solid solution of starting composition $GeS_{0.98}Se_{0.02}$ is less pronounced, but measurable. The deviation of the average values from the nominal concentration of Te and Se in the starting materials is due to slightly different transport properties of the binary components of the mixed systems.

Because of the relative differences in atomic radii between sulfur (S), Se, and Te and because of the individual crystal structures of GeS and GeSe (orthorhombic) and GeTe (rhombohedral), one

TABLE 26-II.—Distribution of Te (A) and Se (B) in Ground-Based and ASTP Space-Grown Crystals

System	Concentration, at.%		
	Average all data	*Average parallel a-axis*	*Average parallel b-axis*
$GeSe_{0.99}Te_{0.01}$ (Ground-based, 2A)	1.83 ± 0.6	2.03 ± 0.5 1.71 ± .6 1.78 ± .4	1.59 ± 0.4 2.07 ± .3 1.81 ± .4
$GeSe_{0.99}Te_{0.01}$ (ASTP, 3A)	1.56 ± 0.1	1.59 ± 0.03 1.52 ± .08 1.56 ± .02	1.58 ± 0.04 1.57 ± .06 1.58 ± .02
$GeS_{0.98}Se_{0.02}$ (Ground-based, 2B)	0.395 ± 0.092	0.371 ± 0.068 .399 ± .061 .399 ± .028	0.374 ± 0.034 .402 ± .020 .422 ± .015
$GeS_{0.98}Se_{0.02}$ (ASTP, 3B)	0.462 ± 0.048	0.470 ± 0.014 .448 ± .020 .470 ± .007	0.459 ± 0.046 .471 ± .009 .463 ± .007

would expect a more homogeneous mixing to occur in the GeS-GeSe system than in the GeSe-GeTe system. Any improvement in the degree of homogeneity as a result of microgravity conditions should thus be more pronounced for GeSe-GeTe than for GeS-GeSe solid solutions. The experimental observations are in agreement with these expectations.

Morphological Characterization of Crystals

Before the microscopic investigation of individual single crystals is discussed, it should be noted that a macroscopic view of the deposition pattern of transport agent (GeI_4) on the system A ampoule walls (fig. 26-5) shows significant differences. The transport agent in the space ampoule (fig. 26-5(a)) is condensed in the form of well-developed, transparent single-crystal platelets and a few needles. The GeI_4 deposition in the ground-based ampoule (fig. 26-5(b)) shows dendritic-type material with a distinct curvature of individual dendrites. The length of these dendrites ranges to approximately 8 mm. The absence of any distinct curvature in the deposition pattern of the space ampoule (fig. 26-5(a)) reflects the more homogeneous gas motion in a microgravity environment.

Optical photomicrographs of representative $GeSe_{0.99}Te_{0.01}$ (A) ground (prototype) and space crystals show qualitative differences in surface morphology, as illustrated in figure 26-6. Most of the prototype crystals (fig. 26-6(a)) reveal ragged edges, intergrowth, and stepped surfaces. The space crystals (fig. 26-6(b)) have smoother surfaces and generally better defined edges. The average dimensions of the ground specimens range from approximately 2 to 8 mm in edge length. The slightly smaller sizes of the space material are in agreement with the lower microgravity transport rates observed for this system (table 26-III).

Optical photomicrographs of representative $GeS_{0.98}Se_{0.02}$ (B) ground (prototype) and space crystals in figure 26-7 reveal distinct morphological differences. The prototype crystals (fig. 26-7(a)) show considerable aggregation, undefined edges, and rough surfaces. The morphological improvement in terms of surfaces and edges of the space crystals is evident from

TABLE 26-III.—Mass Transport Rates Under Ground-Based and Microgravity Conditions

System	*Mass flux, mol/cm²sec*		
	Condition		*Extrapolated diffusion mode*
	Normal gravity	*Microgravity*	
$GeSe_{0.99}Te_{0.01}$ (A)	7.9×10^{-9}	4.2×10^{-9}	1.4×10^{-9}
$GeS_{0.98}Se_{0.02}$ (B)	22.1	22.1	6.5
GeS + Ar (C)	15.0	13.0	2.8

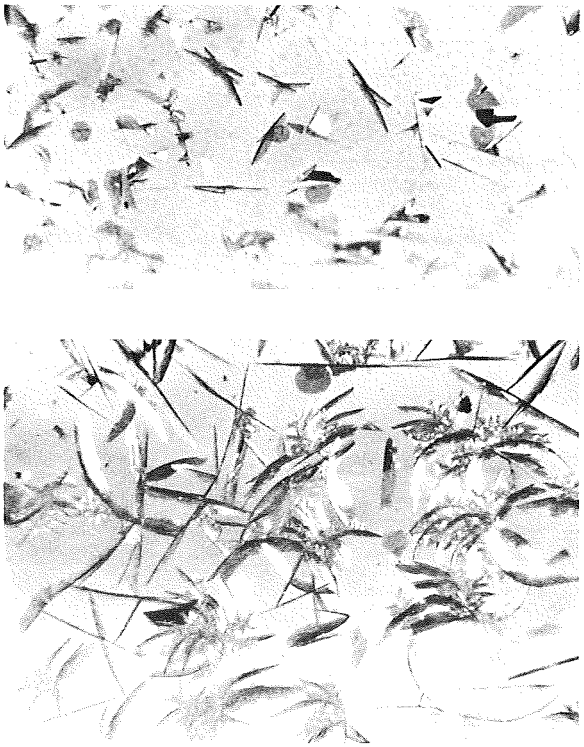

FIGURE 26-5.—Deposition pattern of transport agent GeI_4 (system A) on ampoule walls. (a) In microgravity environment. (b) Under ground-based conditions.

figure 26-7(b). The average dimensions of the space material range from approximately 1 to 7 mm in edge length. Because the system B transport rates (table 26-III) are the same under both ground and space conditions, the external morphological differences reflect the absence of convective interference in a microgravity environment. Similar differences in growth habits were observed for GeS crystals (system C).

The external morphological differences of native faces and edges of typical $GeSe_{0.99}Te_{0.01}$ (A) ground and space crystals are shown in scanning electron photomicrographs in figure 26-8. Rough and partly damaged faces of the ground crystal (fig. 26-8(a)) are contrasted by well-defined surfaces and edges of the space crystal (fig. 26-8(b)). Most of the ground crystals appear to have at least one edge damaged, whereas most of the space crystals have well-developed edges. These results confirm similar observations of the Skylab experiments and indicate homogeneous nucleation, which could occur more frequently under microgravity conditions than on Earth.

Scanning electron photomicrographs of native surfaces of $GeS_{0.98}Se_{0.02}$ (B) ground (prototype) (fig. 26-9(a)) and space (fig. 26-9(b)) crystals reveal significant morphological differences. The degree of surface perfection of the space material (fig. 26-9(b)) is considerably improved compared to the ground specimen (fig. 26-9(a)). Because the transport rates of system B are the same under ground-based and microgravity conditions (table 26-III), the greater crystalline perfection of the space material is attributed to the absence of convective interference.

To investigate the effects of microgravity forces on the degree of crystalline perfection for the bulk of the material, internal faces of ground

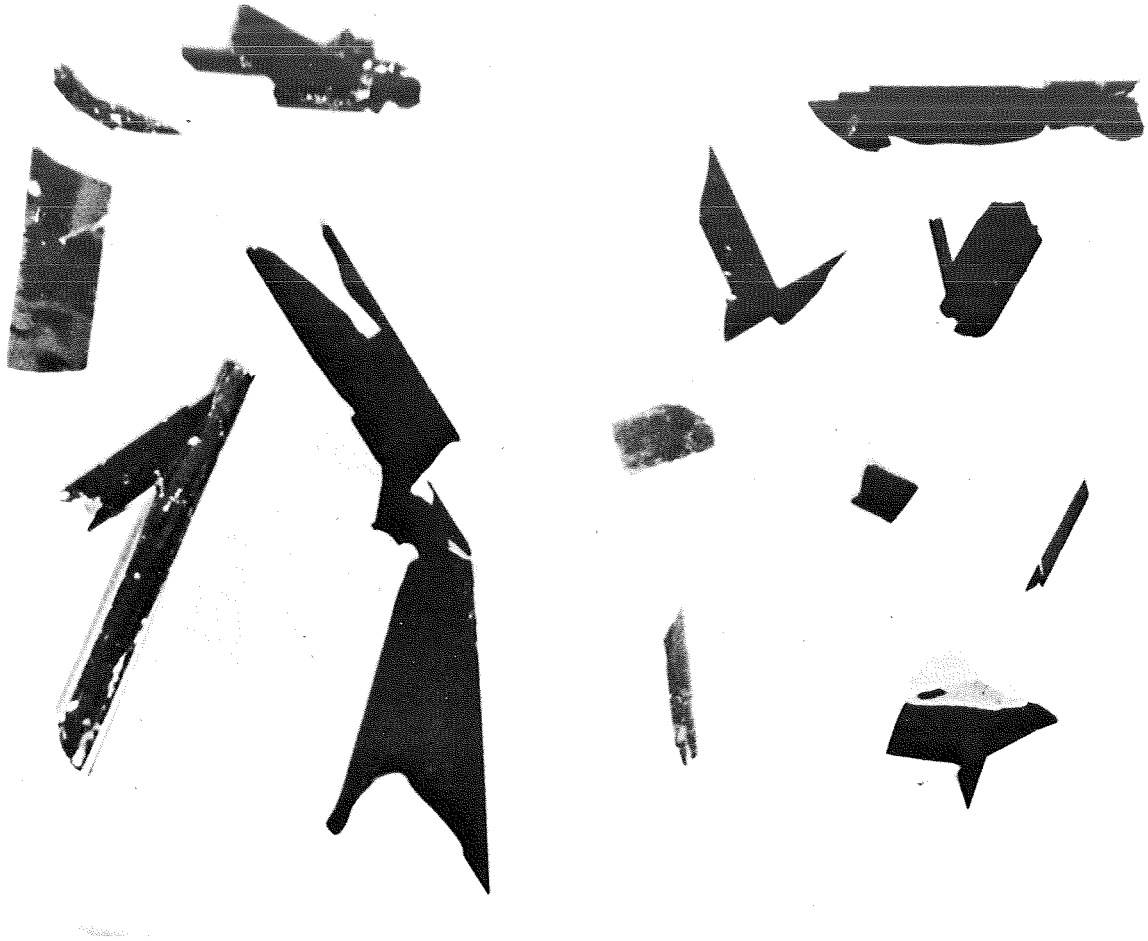

FIGURE 26-6.—Representative crystals of $GeSe_{0.99}Te_{0.01}$ (system A). (a) Ground-based (prototype). (b) Space-grown.

and space crystals were examined by means of chemical etching and optical microscopy. For this purpose, crystal platelets were cleaved parallel to the (001) plane.

An optical photomicrograph of the cleaved face of a ground (prototype) crystal of $GeSe_{0.99}Te_{0.01}$ (system A) shows the presence of large cavities in the bulk of the material (fig. 26-10(a)). After chemical etching, the same area of the crystal is covered with etch pits (fig. 26-10(b)). It is interesting to note that the areas which appear to be mirror smooth at this magnification (fig. 26-10(a)) show a high etch-pit density (fig. 26-10(b)). Etch pits along the walls of the main cavity are also clearly visible. The concentration of etch pits indicates the degree of structural or chemical imperfection in the ground-based material. Similar observations were made for the majority of investigated crystals.

Application of the same cleaving and etching procedures to space-grown crystals of system A yields distinctly different results, as shown in figure 26-11. The photomicrograph of the cleaved crystal reveals that most of the space material is structurally very uniform (fig. 26-11(a)). The photomicrograph after etching of the cleaved space crystal platelet (fig. 26-11(b)) is practically free of etch pits and thus indicates a high degree of microhomogeneity. The line pattern of the crystal, showing (001) planes of different depth with respect to the native surface, is due to cleavage.

Similar differences in etch patterns were observed for ground-based (prototype) and space-grown $GeS_{0.98}Se_{0.02}$ (B) crystals, as shown in

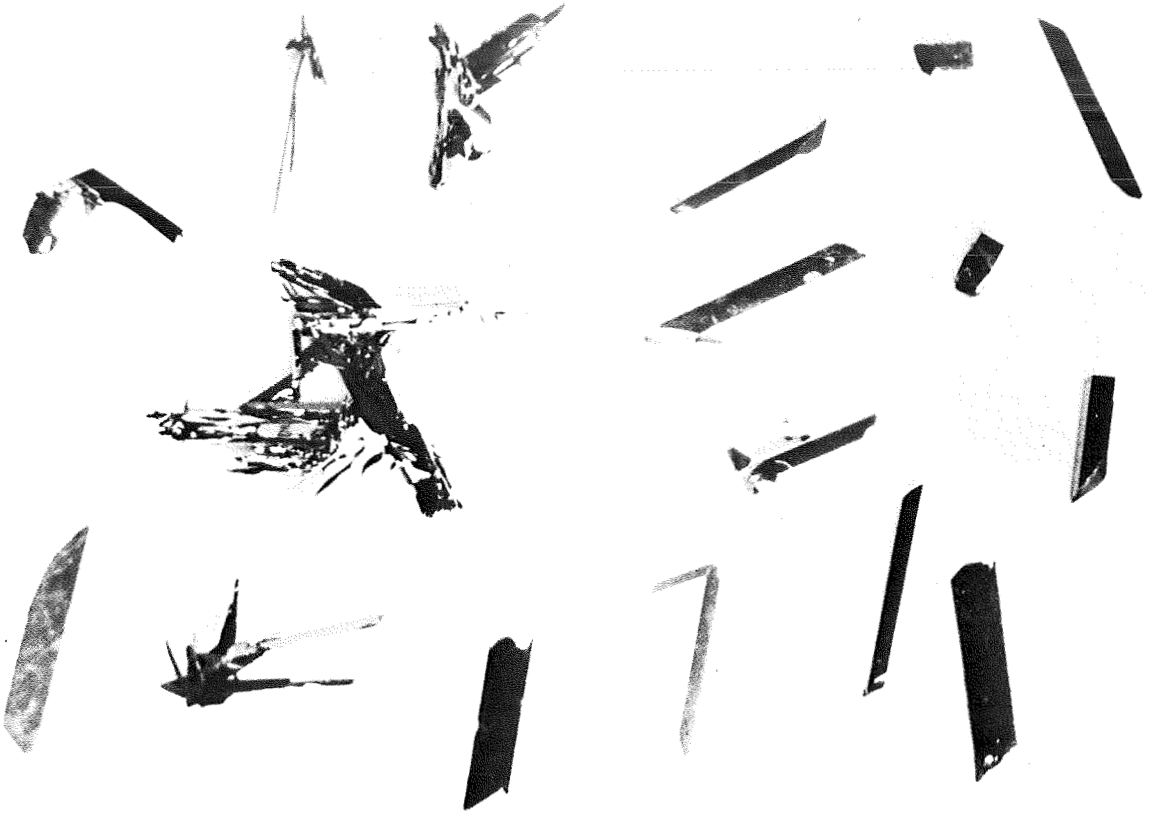

FIGURE 26-7.—Representative crystals of $GeS_{0.98}Se_{0.02}$ (system B). (a) Ground-based (prototype). (b) Space-grown.

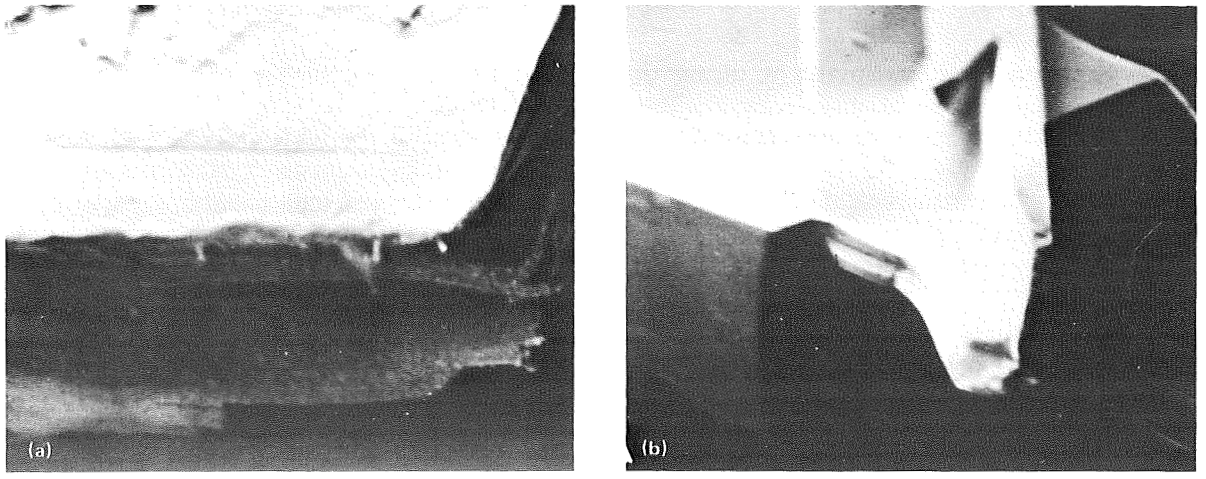

FIGURE 26-8.—Scanning electron photomicrographs (200×) of native faces and edges of $GeSe_{0.99}Te_{0.01}$ (system A) crystals. (a) Ground-based (prototype). (b) Space-grown.

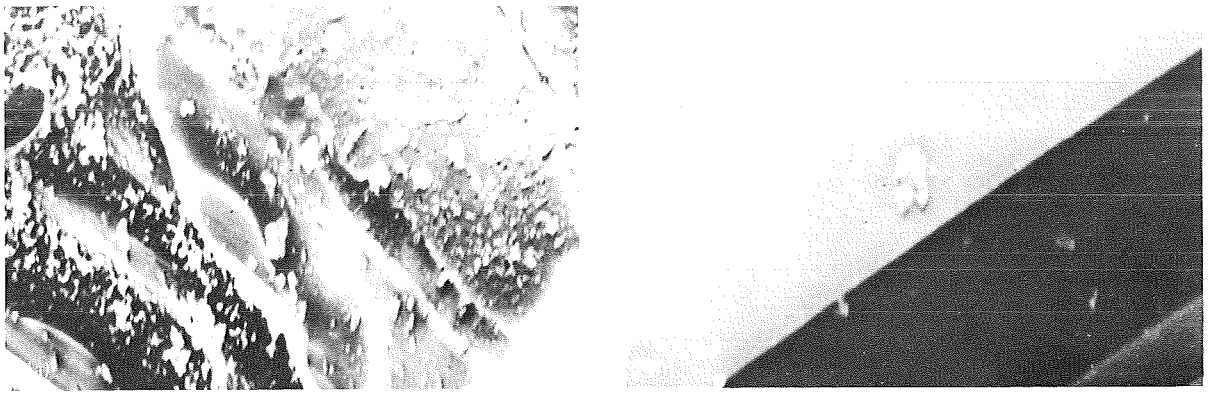

FIGURE 26-9.—Scanning electron photomicrographs (200×) of native faces of $GeS_{0.98}Se_{0.02}$ (system B) crystals. (a) Ground-based (prototype). (b) Space-grown.

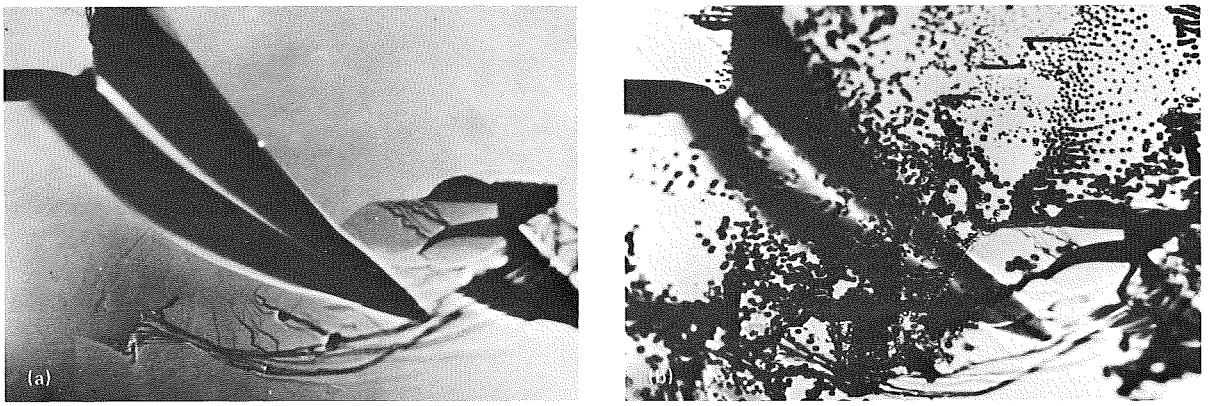

FIGURE 26-10.—Optical photomicrographs (100×) of a cleaved and etched (001) face of a ground-based (prototype) $GeSe_{0.99}Te_{0.01}$ (system A) crystal platelet. (a) Cleaved. (b) Cleaved and etched.

figures 26-12 and 26-13, respectively. For comparative purposes, a ground crystal of above average quality has been selected, as indicated by the cleavage pattern (fig. 26-12(a)). (Most B-type ground crystals contain cavities and elongated channels in the bulk of the material.) Chemical etching of the cleaved (001) face yields large etch pits and lines (fig. 26-12(b)), which are indicative of crystallographic imperfections. This characteristic is in contrast to that revealed by optical photomicrographs of cleaved and etched (001) faces of system B space crystals (figs. 26-13(a) and 26-13(b)). Except for a few isolated etch pits in the crystal plane (fig. 26-13(b)), the bulk of the material is practically unaffected by chemical etching. This characteristic indicates a high degree of crystalline homogeneity of the space-grown material.

Optical photomicrographs of cleaved and etched (001) faces of GeS (C) ground (prototype) and space crystals are shown in figures 26-14 and 26-15, respectively. Whereas the cleaved faces of the prototype (fig. 26-14(a)) and space (fig. 26-15(a)) crystals appear to be of comparable quality, the corresponding etched faces of the ground (fig. 26-14(b)) and space (fig. 26-15(b)) crystals reveal measurable differences. The prototype material shows a high density of etch pits

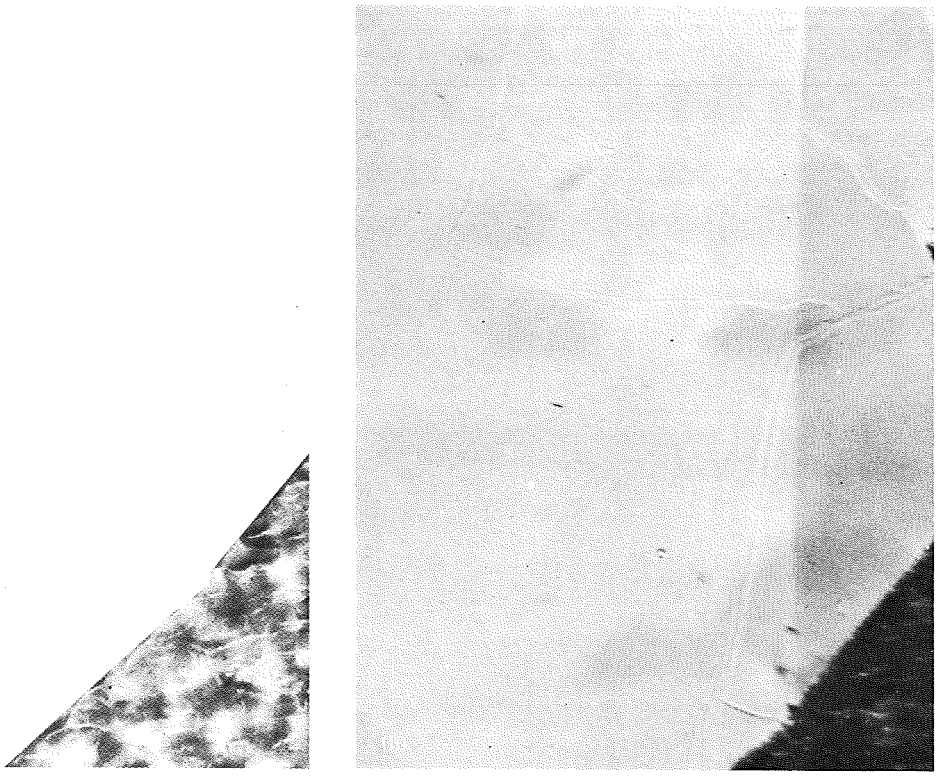

FIGURE 26-11.—Optical photomicrographs (125×) of a cleaved and etched (001) face of a space-grown $GeSe_{0.99}Te_{0.01}$ (system A) crystal platelet. (a) Cleaved. (b) Cleaved and etched.

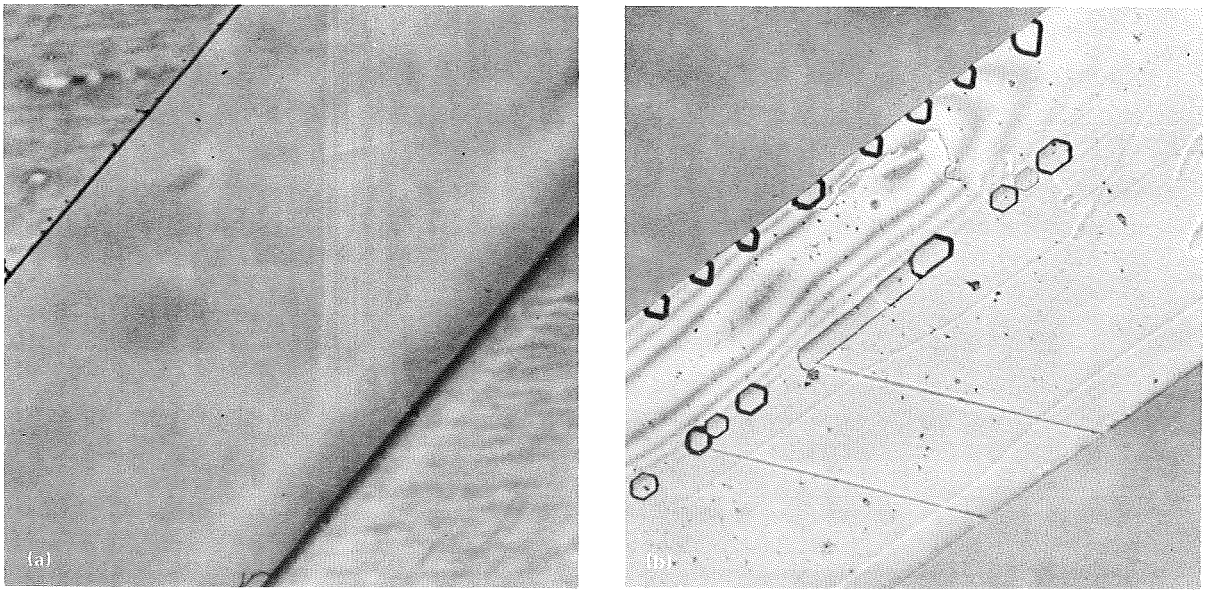

FIGURE 26-12.—Optical photomicrographs (125×) of a cleaved and etched (001) face of a ground-based (prototype) $GeS_{0.98}Se_{0.02}$ (system B) crystal platelet. (a) Cleaved. (b) Cleaved and etched.

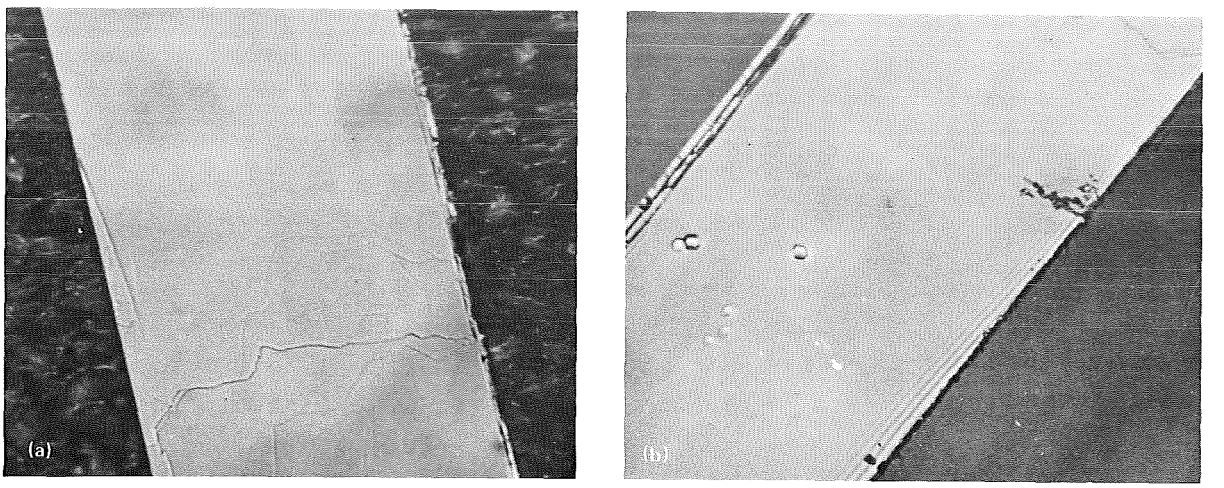

FIGURE 26-13.—Optical photomicrographs (125×) of a cleaved and etched (001) face of a space-grown $GeS_{0.98}Se_{0.02}$ (system B) crystal platelet. (a) Cleaved. (b) Cleaved and etched.

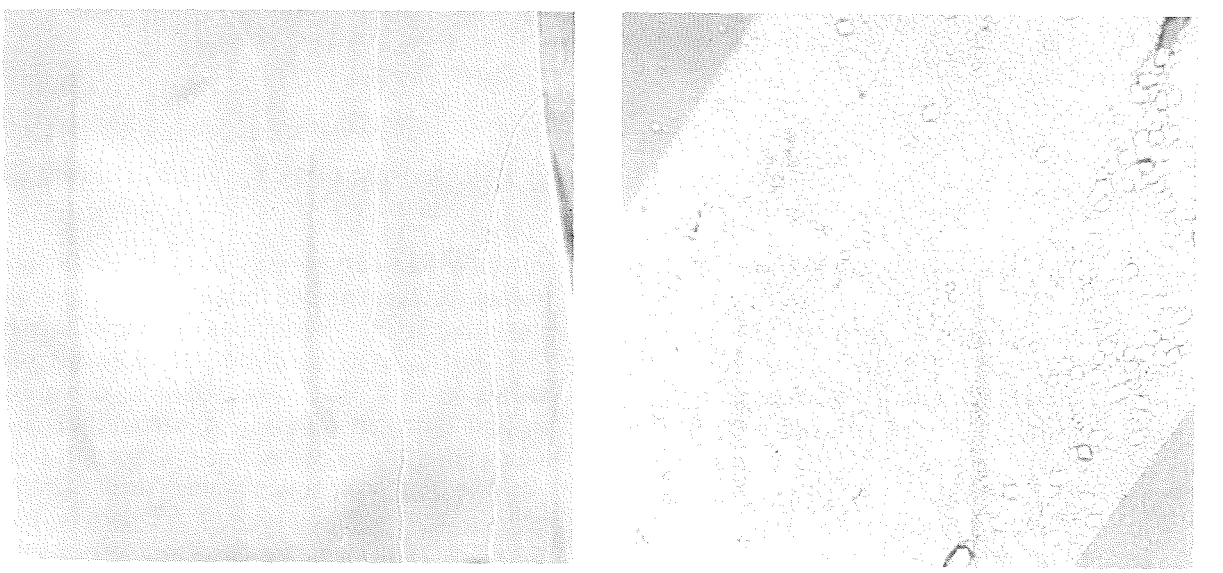

FIGURE 26-14.—Optical photomicrographs (125×) of a cleaved and etched (001) face of a ground-based (prototype) GeS (system C) crystal platelet. (a) Cleaved. (b) Cleaved and etched.

of different sizes (fig. 26-14(b)). The etch pits of the space sample (fig. 26-15(b)) are concentrated in the lower section of the crystal and along the edges, whereas the major part of the plane has a considerably lower pit density than the ground crystal. It was observed that the GeS space crystals (system C) grown in the presence of argon were of slightly lower crystallographic quality than the system A and B space crystals, which were produced in the absence of an inert atmosphere. Studies are in progress to determine whether these differences are due to the incorporation of argon into the GeS lattice.

These differences in cleavage and etch patterns for the three systems were observed for the majority of investigated space and ground crystals. The combined results of the morphological studies demonstrate the considerably improved crystallographic perfection of the crystals grown in a microgravity environment.

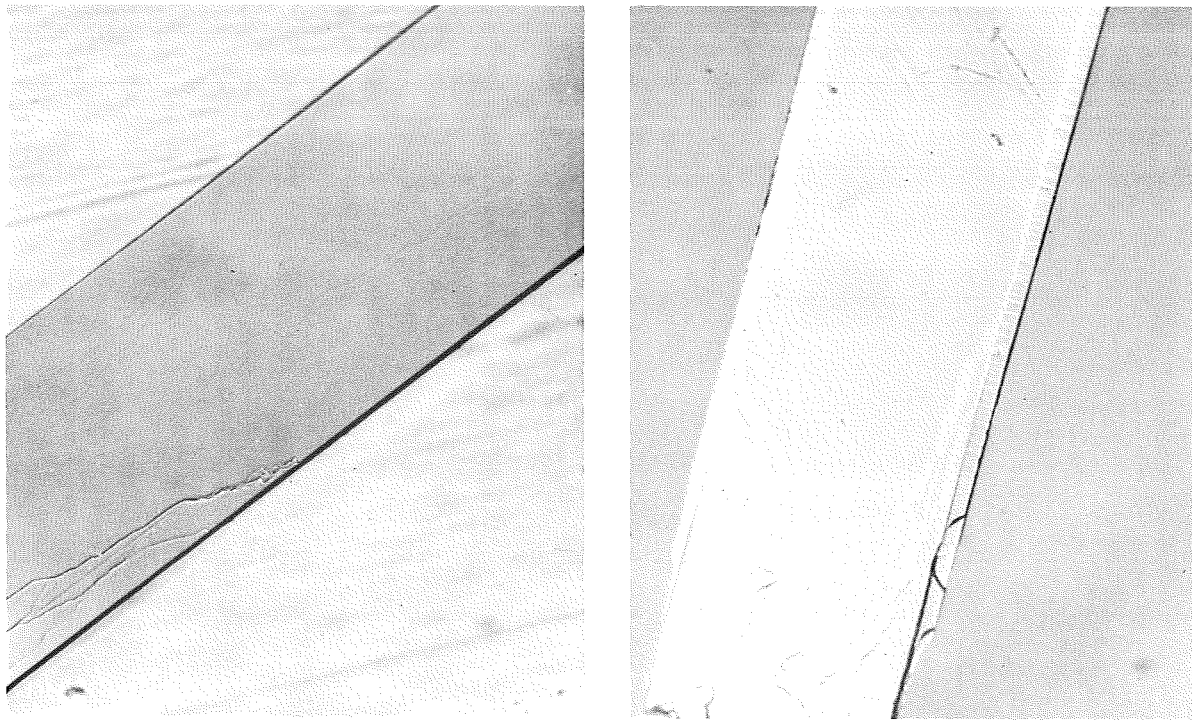

FIGURE 26-15.—Optical photomicrographs (125×) of a cleaved and etched (001) face of a space-grown GeS (system C) crystal platelet. (a) Cleaved. (b) Cleaved and etched.

Mass Transport Rates

The determination of the mass transport rates observed in a microgravity environment is based on the mass of the transported crystals and on the mass loss of the source materials. The same procedures were applied to determine the fluxes of the ground-based (prototype) systems. The experimental uncertainties associated with the recovery of crystals were combined to yield lower values for the mass flux observed under microgravity conditions. The extrapolated values are based on a graphical extrapolation of the diffusion-controlled region of the respective ground-based experimental flux curves shown in figure 26-1. For this purpose, flux as a function of pressure data were plotted in double logarithmic scales and the resulting straight line was extended to the flux corresponding to the pressure employed in the ASTP experiments. This extrapolation is shown for system A in figure 26-16 and for system B and GeS in figure 26-17. The data of the diffusion-controlled region selected for the extrapolation are near the minimum of the individual flux curves (fig. 26-1) to obtain upper values for the predicted fluxes. The extrapolations are based on the assumptions that vapor transport in a microgravity environment is by gas phase diffusion and that other known non-gravity-caused transport effects (e.g., streaming) are included in this procedure. The predicted flux value for system C was obtained analytically from the extrapolated identical values for system B and GeS (fig. 26-17) and the argon pressure in system C, considering the different molecular weights of argon and $GeCl_4$. The mass transport properties of system B and GeS (figs. 26-1 and 26-17) and the transport agent ($GeCl_4$) pressures of systems B and C (95.25 kN/m^2 (0.94 atm) and 97.27 kN/m^2 (0.96 atm), respectively) are the same within limits of error. Therefore, a direct comparison of the effect of argon on the mass flux between systems B and C can be made. In view of the applied evaluation procedures, any differences between observed and predicted (extrapolated) microgravity fluxes are minimized and well outside error limits. The numerical transport results are listed in table 26-III.

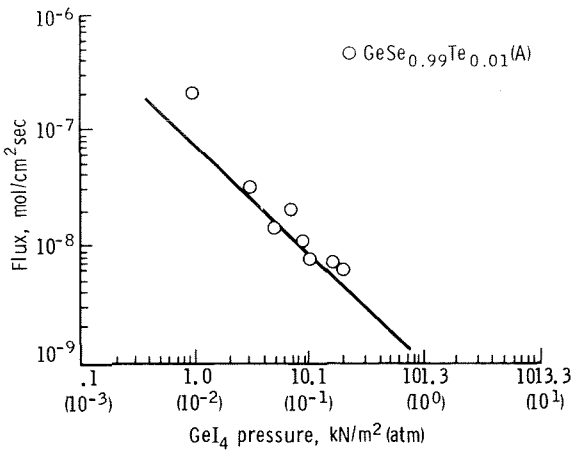

FIGURE 26-16.—Extrapolation of flux as a function of pressure data from the diffusion branch of the ground-based flux curve (fig. 26-1) for system A.

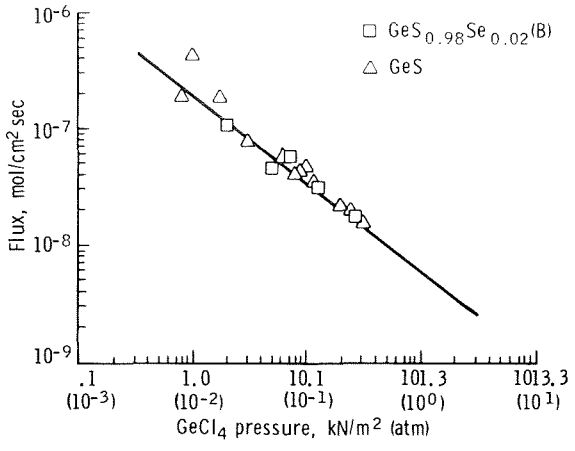

FIGURE 26-17.—Extrapolation of flux as a function of pressure data from the diffusion branch of the ground-based flux curves (fig. 26-1) for system B and GeS.

A comparison of the data in table 26-III reveals a rather significant result. For system A, the microgravity flux is lower than the normal gravity flux but approximately three times greater than predicted for a purely diffusion-type transport. These observations are consistent with the Skylab results. For system B, the normal gravity and microgravity fluxes are the same but the latter is more than three times greater than the transport rate predicted by theory. The pressure of transport agent $GeCl_4$ employed for ASTP system B is different from the GeI_4 pressure of the corresponding Skylab experiment for which the same ground and space fluxes were observed. This fact indicates the importance of the chemical properties of the transport system for flux considerations. For system C, the normal gravity and microgravity fluxes are the same within error limits and the latter is nearly five times greater than predicted. A comparison of the individual flux data of systems B and C demonstrates that the effect of argon on the mass transport rate is the same under normal gravity and microgravity conditions. The observed decrease in flux upon addition of argon is in good agreement with ground-based inert-atmosphere studies, as shown in figure 26-1. These combined results have two important consequences. First, the greater than predicted transport rates observed in a microgravity environment are not caused by gravity fluctuations or any other conditions typical of spacecraft operations. Second, the effect of argon on the mass flux is independent of gravity and, thus, affects the inherent physicochemical properties of the transport system. These observations are of primary importance for the explanation of the unexpected flux results.

In view of the rather unconventional nature of microgravity transport phenomena, it is necessary to demonstrate independently the validity of the discrepancies between the flux values actually observed in space and those predicted on the basis of a diffusion-type transport. For this purpose, different transport models developed by Schaefer (ref. 26-3), Lever (ref. 26-6), Mandel (ref. 26-7), and Faktor et al. (ref. 26-8) have been used. These models are for vapor transport by diffusion and differ essentially in the treatment of the so-called streaming effect or flow factor and in the thermodynamic calculation of partial pressure gradients. Based on these diffusion models, curves of flux as a function of pressure were computed for the temperature gradients and transport agents of the ASTP, Skylab 3, and Skylab 4 experiments. The "theoretical" flux curves were fitted to the diffusion branch of the experimental ground-based curves (fig. 26-1 for the ASTP mission and accordingly for the Skylab missions) to obtain optimal fit. This procedure yielded the numerical constants required for the calculation of the fluxes for the specific ASTP and Skylab conditions. The results of these computations for the different

models are listed in table 26-IV together with the observed and extrapolated fluxes. A comparison of these data shows that the flux values obtained from the model computations agree within a factor of 2 with the extrapolated values. In no case are the transport rates predicted by the models greater than the observed fluxes. When the uncertainties associated with thermodynamic calculations of partial pressures and transport effects are considered, the agreement between the model calculations and the extrapolation data is close. However, because of these uncertainties, the extrapolated data represent the best flux values for comparison. The combined data demonstrate unambiguously that the microgravity transport rates cannot be explained on the basis of an exclusively diffusion-type process. The internal consistency and close agreement between the flux results of the ASTP and Skylab missions obtained for different chemical systems, eight pressures, two transport agents, and three temperature gradients strongly support the validity of these observations. The combined results lead to the conclusion that the greater than predicted mass transport rates in a microgravity environment are due to non-gravity-caused transport effects. These unexpected phenomena are related to thermochemical effects of gas phase reactions, which have not been considered in existing vapor transport models.

The latter conclusion is supported by the analysis and application of models for convective vapor transport on Earth developed by Schaefer (ref. 26-3) based on the Hagen-Poiseuille equation and by Klosse and Ullersma (ref. 26-9) using a hydrodynamic approach and the Navier-Stokes equation. An important difference between these two models is their treatment of the convective boundary layer, the fluid layer immediately in contact with the growing crystal and through

TABLE 26-IV.—Mass Transport Rates Observed and Predicted for Microgravity Conditions

System	*Mass flux, mol/cm²sec*					
	Observed	*Extrapolated*	*Modeled*			
			Schaefer (ref. 26-3)	*Lever (ref. 26-6)*	*Mandel (ref. 26-7)*	*Faktor et al. (ref. 26-8)*
ASTP (877 → 780 K (604° → 507° C)[a])						
$GeSe_{0.99}Te_{0.01}$ (A)	4.2×10^{-9}	1.4×10^{-9}	2.5×10^{-9}	2.7×10^{-9}	2.6×10^{-9}	3.1×10^{-9}
$GeS_{0.98}Se_{0.02}$ (B)	22.1	6.5	8.9	9.1	9.1	9.5
GeS + Ar (C)	13.0	2.8	3.6	3.7	3.2	5.2
Skylab 3 (797 → 695 K (524° → 422° C)[a])						
GeSe (A)	5.0×10^{-9}	0.5×10^{-9}	0.80×10^{-9}	0.89×10^{-9}	0.86×10^{-9}	1.1×10^{-9}
GeSe (B)	10.0	2.5	3.4	3.7	3.6	4.2
GeTe (C)	3.0	.5	.84	.87	.87	.92
Skylab 4 (685 → 619 K (412° → 346° C)[a])						
GeSe (A)	0.8×10^{-9}	0.15×10^{-9}	0.14×10^{-9}	0.14×10^{-9}	0.14×10^{-9}	0.15×10^{-9}
GeSe (B)	1.8	.35	.29	.30	.30	.30
GeTe (C)	1.0	.40	.79	.79	.79	.79

[a]Temperature gradients.

which mass must diffuse. The model based on the Hagen-Poiseuille equation (ref. 26-3) does not include consideration of a boundary layer. In the hydrodynamic model (ref. 26-9), the thickness of the boundary layer depends on the aspect ratio of the enclosure. Preliminary applications of these convection models to the investigators' experimental ground-based flux curves show systematic deviations. The mass fluxes predicted by the first model (ref. 26-3) for convective transport are greater than fluxes observed. The second model (ref. 26-9) agrees with the investigators' experimental results in the initial convection range and predicts fluxes lower than those observed at higher pressures. These deviations from the experimental ground-based data are related to the treatment of the boundary layer in these models (refs. 26-3 and 26-9). In addition, possible thermal effects of gas phase reactions on mass transport and on the boundary layer are not considered in the convection models (refs. 26-3 and 26-9). Theoretical and experimental studies are being conducted to further analyze existing vapor transport models through systematic applications of these models to different transport systems investigated in the RPI laboratory. The immediate purpose of these efforts is the extension of ground-based convection models to agree with experimental results. These modifications combined with the investigators' spaceborne and continued ground experiments will lead to the development of a transport model for microgravity conditions.

On the basis of these results, the transport phenomena observed for the ASTP and Skylab mission experiments are of far-reaching scientific and technological significance. The improvement of ground-based transport models is of basic and practical value for crystal growth theories and techniques on Earth. A transport model for space conditions based on microgravity experiments is of primary importance for actual space-processing applications.

SUMMARY AND CONCLUSIONS

The original objectives of the crystal growth by vapor transport experiment were to investigate the effects of microgravity forces on the morphology of single crystals of mixed systems and to determine the mass transport rates of these systems using the chemical transport technique. For this purpose, three vapor transport experiments were performed during the Apollo-Soyuz mission using three chemical compounds, two transport agents, and one inert gas in one common temperature gradient. The analysis of these experiments is based on a direct comparison of X-ray diffraction, microprobe, scanning electron and optical microscopy, and chemical etching studies of crystals obtained under ground-based (prototype) and microgravity conditions. The results demonstrate a considerable improvement in structural and chemical homogeneity, surface morphology, and bulk perfection of the space-grown materials compared to ground-based specimens. In addition to the positive crystallographic results, the confirmation of greater mass transport rates in microgravity than predicted by existing transport models represents the second major achievement of this experiment.

The excellent agreement between the ASTP and Skylab results demonstrates the validity of the observed crystal growth and transport properties in space for a class of technologically useful materials. This confirms the initial predictions concerning the suitability of the vapor transport technique for the growth of higher quality crystals and for the observation of unexpected phenomena in a microgravity environment. These results are of basic scientific and practical importance for the modification of transport models on Earth. The production of high-quality crystals at high mass transport rates is of technological significance for space-processing applications.

REFERENCES

26-1. Wiedemeier, H.; Klaessig, F. C.; Wey, S. J.; and Irene, E. A.: Vapor Growth of GeSe and GeTe Single Crystals in Micro-Gravity. Proceedings of the Third Space Processing Symposium on Skylab Results, vol. 1. June 1974, pp. 235-256.

26-2. Wiedemeier, Heribert; Klaessig, Frederick C.; Irene, Eugene A.; and Wey, Song J.: Crystal Growth and Transport Rates of GeSe and GeTe in Micro-Gravity Environment. J. Crystal Growth, vol. 31, Dec. 1975, pp. 36-43.

26-3. Schaefer, Harald: Chemical Transport Reactions. Academic Press (New York), 1964.

26-4. Wiedemeier, H.; Irene, E. A.; and Chaudhuri, A. K.: Crystal Growth by Vapor Transport of GeSe, $GeSe_2$, and GeTe and Transport Mechanism and Morphology of GeTe. J. Crystal Growth, vol. 13-14, 1972, pp. 393-396.

26-5. Wiedemeier, H.; and Irene, E. A.: The Chemical Transport Rates and Crystal Morphology of GeSe. Z. Anorg. Allgem. Chem., vol. 400, 1973, pp. 59-66.

26-6. Lever, R. F.: Multiple Reaction Vapor Transport of Solids. J. Chem. Phys., vol. 37, no. 5, Sept. 1, 1962, pp. 1078-1081.

26-7. Mandel, G.: Multiple Reactions and the Vapor Transport of Solids. J. Chem. Phys., vol. 37, no. 6, Sept. 15, 1962, pp. 1177-1180.

26-8. Faktor, M. M.; Garrett, I.; and Heckingbottom, R.: Diffusional Limitations in Gas Phase Growth of Crystals. J. Crystal Growth, vol. 9, May 1971, pp. 3-11.

26-9. Klosse, K.; and Ullersma, P.: Convection in a Chemical Vapor Transport Process. J. Crystal Growth, vol. 18, Jan.-Mar. 1973, pp. 167-174.